Numerical results from different variational theories of fracture

Giovanni Lancioni
Università Politecnica delle Marche, Dipartimento di Architettura, Costruzioni e Strutture, Ancona, Italy
g.lancioni@univpm.it

ABSTRACT. Four different variational models of fracture are considered. They are numerically implemented by means of a self-made finite element code and the crack evolution in a fiber-matrix composite body is simulated. The different results are compared.

KEYWORDS. Fracture mechanics; Variational calculus; Finite elements; Energy methods.

INTRODUCTION

The equilibrium problem for brittle elastic bodies was formulated in a variational format in [1]: the equilibrium configuration is that which minimizes an energy functional given by the sum of a bulk energy and a surface energy. The surface term is proportional to the area of the fracture surface, just as in Griffith's theory of fracture.
The resulting problem is a free discontinuity problem, since the crack surface is unknown. It is numerically solved by making use of special finite elements such as boundary elements or extended finite elements, which account for the displacement discontinuities. An alternative numerical approach was followed in [2], where a regularized functional, which approximates the starting energy in the sense of gamma-convergence, was considered. In this functional the jump of the displacement field at the fracture surface is approximated by a smooth scalar field which plays the rule of a "damage" field, and the corresponding minimum problem is solved numerically by means of the standard finite elements method. The sharp fracture of the original problem is approximated by a smeared crack in the numerical model. Moreover, if a loading parameter is monotonically increased, the evolution problem can be taken into account by considering a further irreversibility condition which prevent the crack healing. This condition must be satisfied within each loading step of the incremental numerical scheme.
In this paper we consider the regularized problem and formulate four models by assigning four different expression to the bulk term of the energy.

i. *Nonlinear model*, proposed in [3], which assumes the stored energy density of an Ogden material, typical of finite elasticity, in the bulk term.
ii. *Linear model*, proposed in [2], where the bulk energy is a quadratic function of the displacement gradient, just as in infinitesimal elasticity.
iii. *Shear model*, proposed in [4], where the bulk term is split into its hydrostatic and deviatoric parts and only the deviatoric part is engaged in the energetic competition with the fracture term to incorporate the idea of a less brittle "deviatoric-type" fracture.
iv. *Linear combined model*, proposed independently in [5] and [6], where the linear model is considered when the material volume change is positive and the shear model is considered when the volume change is negative. This last model reproduces cleavage fracture in tensile tests and mode II fracture in compression tests.

The four models are numerically implemented and some simulations are performed to reproduce the fracture evolution in a composite body constituted by an unbreakable fiber and a breakable matrix. The results are compared.

THE MODELS

Four different variational models are considered which differ only for the shape of the bulk term in the energy functional. The four energies are described in the following.

The non-linear model [3]

The first energetic functional to be considered is

$$E_{nl}(f,s)=\int_B \left(s^2(x)+k_\varepsilon\right)W_{nl}\left(\nabla f(x)\right)dx+\frac{\gamma}{2}\int_B\left(\varepsilon\left|\nabla s(x)\right|^2+\frac{1}{\varepsilon}\left(1-s(x)\right)^2\right)dx \qquad (1)$$

where the first integral represents the bulk energy and the second integral is the fracture energy. The functional unknowns are the deformation field f and the fracture field s, and they are defined in suitable Sobolev spaces. The field s takes values close to 0 near the crack and close to 1 away from it. The coefficient γ is the fracture toughness and ε is a mathematical term such that, when it goes to zero, the regularized problem converges to the Griffith-like problem studied in [1]. We refer to [3] for details on the convergence questions. The term ε has a physical meaning as well: it represent the intrinsic material length scale, measuring the thickness of the process zone [4]. The small parameter k_ε is of order $o(\varepsilon)$ and was introduced to render coercive the functional. We assign to the elastic energy density the expression

$$W_{nl}(\mathrm{F})=\frac{\mu}{2}\left(\left|F\right|^2-3\right)+\frac{1}{2}\lambda\left(\log\left(det\,F\right)\right)^2-\mu\log\left(det\,F\right) \qquad (2)$$

proposed in [8] for an isotropic, compressible neo-Hookean material [7]. The coefficients μ and λ are the Lamè coefficients. The energy density is such that $W_{nl}(\mathrm{F})\to\infty$ as $det\,F\to 0$ and $det\,F\to\infty$ to avoid extreme deformations.

When (1) is minimized, a competition is engaged between the first integral term, the elastic bulk strain energy, and the second integral, the fracture energy. The strain energy is minimized for fixed f by $s = 0$, while the fracture energy is minimized by s=1. But the transition from $s = 1$ to $s = 0$ is associated with a ∇s which is penalized by the first term in the second integral, which represents an interface energetic term.

The linear model [2]

The second energetic functional, proposed in [2], assumes that the strain energy density is a quadratic form of the displacement gradient, like in the theory of infinitesimal elasticity. The energy for an isotropic material is

$$E_l(u,s)=\int_B\left(s^2(x)+k_\varepsilon\right)\left(\mu\left|sym\nabla u\right|^2+\frac{\lambda}{2}\left(div\,u\right)^2\right)dx+\frac{\gamma}{2}\int_B\left(\varepsilon\left|\nabla s(x)\right|^2+\frac{1}{\varepsilon}\left(1-s(x)\right)^2\right)dx \qquad (3)$$

where u is the displacement field. We notice that , and thus both in a tension test and in a compression test, which differ only for the displacement sign, the fracture field is the same. Moreover, there is no control on the volume change and phenomena of interpenetration can occur.

The shear model [4]

The third functional, introduced in [4], is

$$E_s(u,s)=\int_B\left(s^2(x)+k_\varepsilon\right)W_{dev}(u)+\left(1+k_\varepsilon\right)W_{sph}(u)\,dx+\frac{\gamma}{2}\int_B\left(\varepsilon\left|\nabla s(x)\right|^2+\frac{1}{\varepsilon}\left(1-s(x)\right)^2\right)dx \qquad (4)$$

where W_{dev} and W_{sph} are the deviatoric and spherical parts of the strain energy density of a linearly elastic isotropic material, that is,

$$W_{dev}(u)=\mu\left(\left|sym\nabla u\right|^2-\frac{1}{3}\left(div\,u\right)^2\right),\quad W_{sph}(u)=\left(\frac{\mu}{3}+\frac{\lambda}{2}\right)\left(div\,u\right)^2 \qquad (5)$$

If the functional (4) is minimized, only the deviatoric part of the strain energy is engaged in the energetic competition with the fracture term since only the deviatoric part multiplies the fracture field s, while the hydrostatic part is unaffected by the fracture. As a result, only the deviatoric deformation is associated with the fracture: micro-fractured shear bands forms and coalesce in mode II cracks, according to the von Mises-Hencky-Huber criterion of local failure. The modification in

(4) is possible since the deviatoric and spherical parts of the strain energy decompose additively. Such a decomposition is not possible if finite elasticity is considered like in the functional (1). This functional is symmetric: $E_s(u,s) = E_s(-u,s)$.

The combined model [5,6]

This last functional [5,6] combines the functionals (3) and (4) as follows:

$$E_s(u,s) = \int_B H(u,s)\,dx + \frac{\gamma}{2}\int_B \left(\varepsilon |\nabla s(x)|^2 + \frac{1}{\varepsilon}(1-s(x))^2 \right) dx \tag{6}$$

with

$$H(u,s) = \begin{cases} \left(s^2(x)+k_\varepsilon\right) W_{dev}(u) + (1+k_\varepsilon) W_{sph}(u), & if \quad div\, u < 0 \\ \left(s^2(x)+k_\varepsilon\right)(W_{dev}(u) + W_{sph}(u)), & if \quad div\, u < 0 \end{cases} \tag{7}$$

It assumes different bulk energies, depending on the sign of the material volume change. If the volume change is positive, that is, the material expands like in a traction test, then the energy functional has the expression (3) which accounts for cleavage cracks. Differently, if the material reduces its volume like in a compression test, the energy has the form (4), which is tailored to predict mode II cracks. It follows a different material behavior under traction and compression. Moreover, if the crack opens under compression, the cracked zone preserves elastic sources due to the spherical strain energy unaffected by the fracture. It was proved in [5] that, if the functional (6) is assumed, material interpenetration is avoided in the limit case $\varepsilon \to 0$.

The numerical scheme for the evolutionary problem

The functionals (1), (3), (4) and (6) are numerically minimized by means of a self-made finite element code developed in Matlab. Triangular elements with linear shape functions are used. The minimization is performed through an iterative scheme which, at each step, minimizes the functional in two times: it looks for the minimizing displacement, keeping the fracture fixed, and then for the minimizing fracture, for fixed displacement (see [2- 5] for the details).

The evolutionary problem is numerically solved as follows. On the body boundary portion ∂B_u is assigned the displacement

$$u(x,t) = t\bar{u}(x), \qquad on\ \partial B_u$$

with $\bar{u}$ an assigned displacement and $t \in (0, t_{final})$ a loading parameter, improperly called time, which is increased in a discrete way. Let δt be the loading increment at each time step. At each increment of the assigned displacement the irreversibility condition

$$s(x,t+\delta t) \le s(x,t)$$

must be satisfied to prevent crack healing.

The numerical code includes a mesh refinement which automatically subdivides into sub-elements those elements at which the values of s become smaller than a given threshold (s=0.8 in the following simulations).

SIMULATIONS

The mechanical behavior of specimens constituted by an elastic unbreakable fiber surrounded by a breakable matrix is reproduced. Both compression and traction tests are performed. The above four models are implemented and their results are compared. The hypothesis of plane strain state is assumed.

Geometry and material properties

The geometry is represented in Fig. 1. The boundary conditions are

$$u = 0,\ s = 0 \quad on\ AB$$

$$u = te_2,\ s = 0 \quad on\ CD$$

$$Tn = 0,\ \nabla s \cdot n = 0 \quad on\ AC\ and\ BD$$

with T the stress tensor and n the outward normal tensor. The material properties are defined per unit thickness. The matrix is characterized by $\mu = \lambda = 2.2 \cdot 10^6 N/cm$, $\gamma = 10^4 N$, and the fiber by $\mu = \lambda = 3.3 \cdot 10^6 N/cm$, $\gamma = \infty$ (unbreakable).

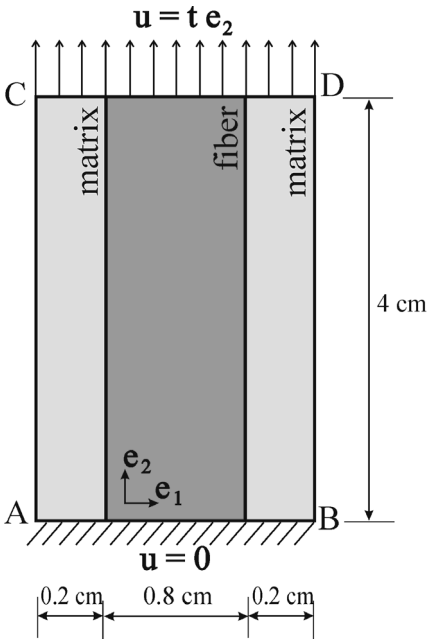

Figure 1: Geometry.

Moreover, we assign $\varepsilon = 10^{-1} cm$ and $k_\varepsilon = 10^{-2}$.

Numerical results

In Fig. 2 the fracture energy (dark gray line), the bulk energy (light gray line) and the total energy (black line) of the matrix are plotted as a function of the vertical displacement t imposed on the upper side of the specimen. The values of t are positive in a traction test and negative in a compression one. The solid lines in Fig. 2 correspond to the nonlinear model, the dashed lines to the linear model (considered only in the traction test) and the dotted lines to the shear model (considered only in the compression test). Only the traction and compression tests are considered for the linear and shear models respectively, because they are symmetric (see Sects. *The linear model*, *The shear model*). Since in a traction test $div u(x) \geq 0, \forall x$, the combined model coincides with the linear model for $t \geq 0$. On the contrary, since in a compression test $div u(x) \leq 0, \forall x$, then the combined model coincides with the shear model for $t \leq 0$. Thus the dashed and dotted curves are also that of the combined model.

Let us analyze the results given by the nonlinear model. First of all we notice a completely different behavior under tension and under compression. In a traction test, the crack evolves as follows. First, three cracks form, two on the left side and one on the right side, as shown in Fig. 3.1. When they open, the bulk and fracture energies take a first jump. Then a fourth crack opens on the right side as depicted in Fig. 3.2. Its formation corresponds to the second energies jump. Finally a fifth crack appears at t = 0.45 on the right side (Fig. 3.3). The fractures are about equidistant in the longitudinal direction and alternates their position on the right and left sides. It follows that the final cracked configuration is that represented in Fig. 5.1: the specimen is stretched and the central fiber assumes the shape of a snake, whose bending concavity is opposite to the crack position (a crack on the left produces a bending whose concavity is oriented on the right, and vice versa). In a compression test, first a diffuse crashed area forms in the middle of the right string (Fig. 4.1) at t = -0.28, and then two further crashed areas appear on the left side (Fig. 4.2). The first and the second crack openings occur at values of t very close each other which corresponds to the jumps in the energies curves. The specimen exhibits a smaller resistance to compression than to tension. It is due to the fact that a buckling phenomenon takes place in the compression test as shown by the deformed configuration of Fig. 5.2.

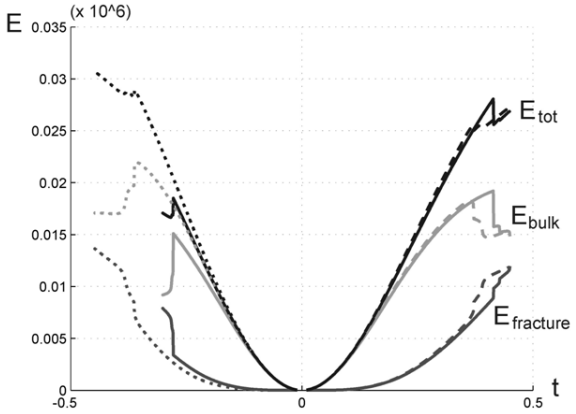

Figure 2: Energies versus t.

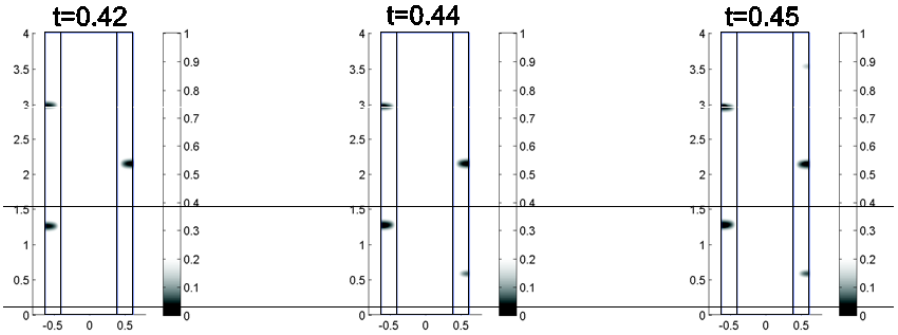

Figure 3: Nonlinear model. Fracture field in a traction test.

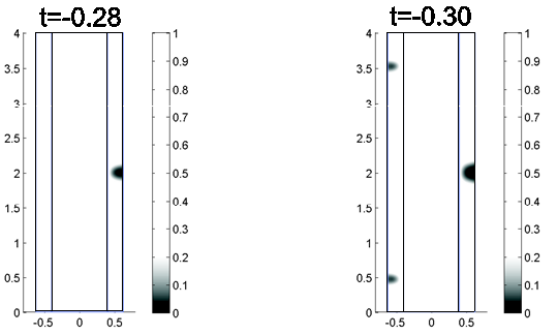

Figure 4: Nonlinear model. Fracture field in a compression test.

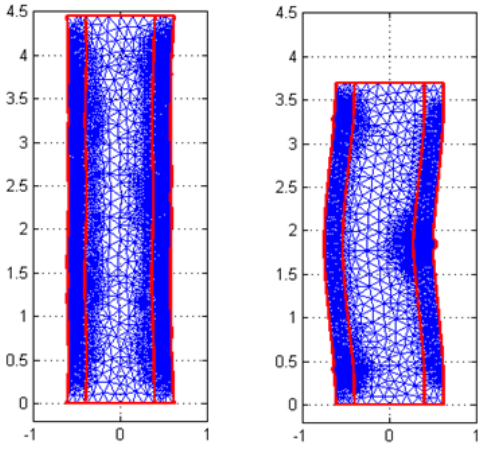

Figure 5: Nonlinear model.
Actual configuration at t=0.45 (traction test) and t=-0.30 (compression test).

For the combined linear model the fracture fields under compression and traction are plotted in Fig. 6. Only three fractures open in both the two cases. The crack regions are wider in compression than in traction. It is due to the fact that sloped shear fractures open under compression (in this case the combined model coincides with the shear model). However they are not evident in Fig. 6.1 since the matrix strips are too narrow. The cracks produce the expulsion of material. On the contrary, thinner cuts due to cleavage fractures form under traction (in this case the combined model coincides with the linear model). If the energies curves of Fig. 2 are compared, we notice that the combined model overestimates the material strength in tension since it does not penalize the spherical stain energy, and it underestimates the material sources under traction.

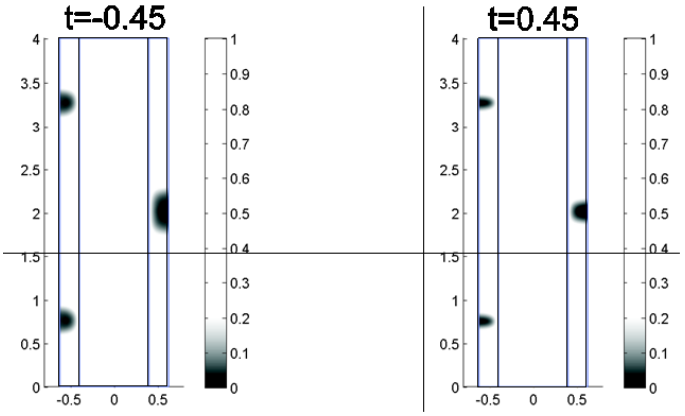

Figure 6: Linear combined model. Fracture field.

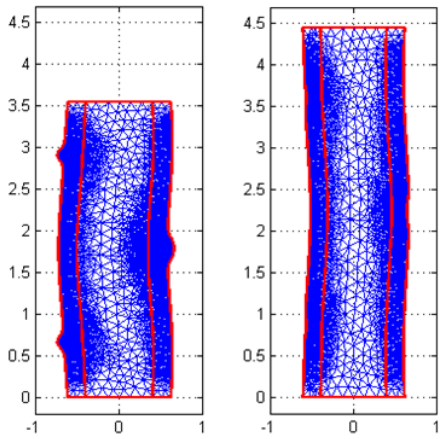

Figure 7: Linear combined model. Actual configuration at t=-0.45 and t=0.45.

CONCLUSION

Four different numerical models for fracture are tested by comparing their predictions on the breaking of a fiber-matrix composite body. The combined model joins the capabilities of the linear and shear models, by accounting for both mode I and mode II fracture. It predicts cleavage fracture when the material is compressed and shear fracture when it is stretched. However it does not solve the problem of material interpenetration which occurs when shear and compression deformations coexist. The nonlinear model forbids material interpenetration by introducing a suitable energetic barrier, and it predicts not-symmetric behaviors as well. However it requires a greater computational effort in terms of code complexity and computing time.

The combined model is suitable for quasi-brittle materials, which exhibit shear fracture mechanisms and have large strength sources due to micro-grain friction under compression. The nonlinear model, on the other hand, is suitable for ductile materials which undergo large deformations before they break.

REFERENCES

[1] G.A. Francfort, J.J. Marigo, J. Mech. Phys. Solids, 46 (1998) 1319.
[2] B. Bourdin B., G.A. Francfort, J.J. Marigo, J. Mech. Phys. Solids, 48 (2000) 797.
[3] G. Del Piero, G. Lancioni, R. March, J. Mech. Phys. Solids, 55 (2007) 2513.
[4] G. Lancioni, G. Royer-Carfagni, J. Elast, 95 (2009) 1.
[5] H. Amor, J.-J. Marigo, C. Maurini, J. Mech. Phys. Solids, 57 (2009) 1209.
[6] F. Freddi, G. Royer-Carfagni, In: XIX Congresso AIMETA, Ancona (2009).
[7] R.W. Ogden, Non-linear elastic deformations. Ellis Horwood, Chichester, UK (1984).
[8] J.C. Simo, K.S. Pister, Comput. Methods Appl. Mech. Eng., 46 (1984) 201.